Available online at www.sciencedirect.com

ScienceDirect

Procedia Engineering 108 (2015) 332 – 339

Procedia Engineering

www.elsevier.com/locate/procedia

7th Scientific-Technical Conference Material Problems in Civil Engineering (MATBUD'2015)

Studies on the effect of a limited polarization range of reinforcement on impedance spectra shapes of steel in concrete

Mariusz Jaśniok[a,*]

[a] *Department of Building Structures, Silesian University of Technology, Akademicka 5, 44-100 Gliwice, Poland*

Abstract

Polarization tests by impedance spectroscopy were conducted on single rebars in rectangular concrete specimens. Five different polarized areas of reinforcement were determined by means of an insulation tape on steel bars. The tests were conducted on two series of concrete specimens, with and without chlorides. The tests indicated a very clear effect of spectra "scaling" in a function of the change in reinforcement polarization area. The observed phenomenon was explained on the basis of the original 3D model of steel–concrete system.

Peer-review under responsibility of organizing committee of the 7th Scientific-Technical Conference Material Problems in Civil Engineering

Keywords: reinforced concrete; reinforcing steel; corrosion; EIS; electrochemical impedance plots; current lines; tests; model

1. Introduction

This paper focuses on an issue that is related to a widely understood diagnosis of reinforced concrete structures and corrosion tests carried out on them (Jaśniok et al. [7], Jaśniok and Jaśniok [9], Jaśniok et al. [10]). Three polarization techniques: Linear Polarization Resistance, Galvanostatic Pulse Method, and Electrochemical Impedance Spectroscopy perform well for the purpose of the advanced corrosion measurements in reinforced concrete. The latter (EIS) is the most difficult for interpretation, but it provides the most in-depth evaluation of

* Corresponding author. Tel.: +48 32 237 2265; fax: +48 32 237 1127.
E-mail address: mariusz.jasniok@polsl.pl

Peer-review under responsibility of organizing committee of the 7th Scientific-Technical Conference Material Problems in Civil Engineering
doi:10.1016/j.proeng.2015.06.155

corrosion in reinforced concrete because this technique covers electrochemical properties of both steel and concrete (Feliu et al. [2], Ford et al. [3]).

The greatest problem referring to the proper interpretation of polarization tests on steel in concrete is related to unknown, because covered with concrete, the polarized area of reinforcement A_p (described as the polarization range L_p in Figs 1÷4). The defined area is necessary for interpreting the measured electrochemical characteristics with reference to the working electrode active area. For many years, the tests on this issue have been focused on an attempt to control the distribution of polarization currents in concrete – Fig. 1a (Gonzalez et al. [4]). While measuring impedance of the reinforced concrete element, alternating current is flowing between the counter electrode *1* and the working electrode *2* (a steel bar). The reference electrode *3* is the third electrode in the system, and the potentiostat *4* monitors the measurement course.

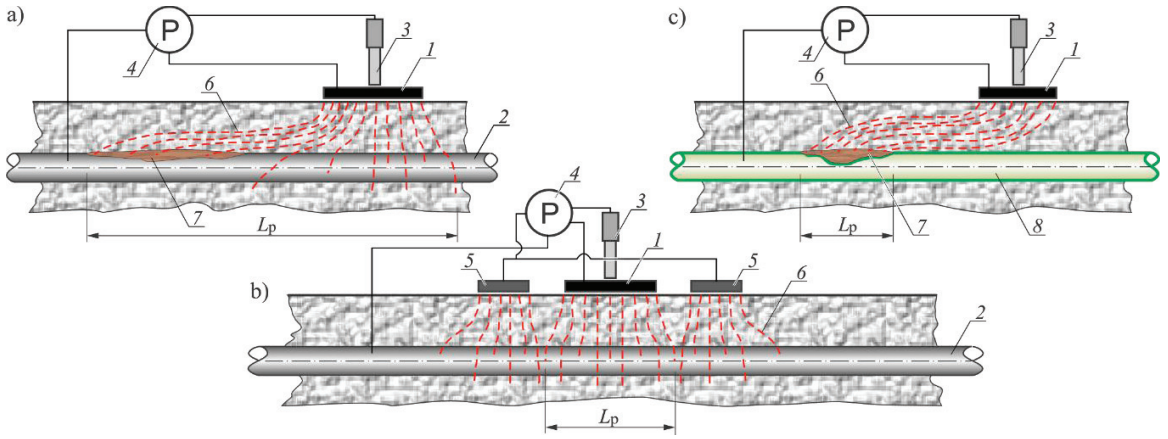

Fig. 1. A distribution of current lines in concrete during reinforcement polarization: a) an effect of local polarization cell (Gonzalez et al. [4]), b) polarization limited by the guard ring (Feliu et al. [1]), c) an effect of damaged epoxy coating of the reinforcement.

The additional reference electrode *5* (so called the guard ring – Fig. 1b) described in the papers (Lemoine et al. [11], Matsuoka et al. [13]) was intended to restrict the distribution of polarization currents *6* to the specified area defined by the range L_p. The guard ring technique performs quite well for uniform corrosion of steel (Fig. 1b), whereas the current flow beyond the area limited by the guard ring can be difficult to estimate for passivated steel (Feliu et al. [1]). It should be also mentioned that the distribution of polarization currents between the counter electrode and the reinforcement can be influenced not only by the electrochemical state of steel area, but also non-uniform moisture content in concrete and local corrosion cells. A problem on identifying local corrosion in concrete-coated reinforcement is one of the most difficult issues related to diagnosing reinforced concrete corrosion (Macdonald et al. [12]). The mentioned guard ring technique has been completely unreliable for local corrosion. Therefore, this paper describes an attempt to test the artificially forced concentration of polarization currents by analogy with the phenomenon of attracting current lines by local corrosion cells (Fig. 1a). To make it more precise, the tests consisted in simulating a corrosion cell *7* in a place of the damaged epoxy coating *8* used as one of reinforcement protections against corrosion – Fig. 1c (Saravanan et al. [14]). The effect of concentrated current lines *6* on different areas of the polarized reinforcement was obtained by means of the insulation tape put on steel rebars before placing concrete mix. The tests were carried out by impedance spectroscopy to relate the impact of limited polarized area not only to electrochemical characteristics of steel, but also to electrochemical properties of concrete.

2. Course of tests

The impedance tests were conducted on 10 concrete test elements reinforced with a single steel rebar. The specimens were prepared in two series *S1* and *S2* – 5 pieces in total. Concrete mix with w/c ratio = 0.43, per 1 m^3

of concrete was composed of: 489 kg of Portland cement 32.5R; 501 kg of fine aggregate with the fraction up to 2 mm; 1168 kg of coarse aggregate with the fraction of 2÷8 mm and 212 litres of water. For *S2* series, 2% $CaCl_2$ related to cement mass in concrete was added to the concrete mix. The specimens were prepared in a rectangular shape, with dimensions of 250×100×100 mm. Each specimen *1* contained identical steel bars *2* made of smooth steel of S235JR grade, with a diameter of ϕ = 16 mm (Fig. 2a). The cover was assumed to be constant c = 20 mm, for all test elements. To force diversified polarized areas *3* during the tests, each bar was peripherally covered with the insulation tape *4*. Five versions of the polarized area (identical for each *S1* and *S2* series) were assumed. They were located symmetrically to the midpoint of each bar length (Fig. 2b). At the constant bar diameter, the working electrode active areas only differed in the length of polarized range of the reinforcement L_p = 50, 100, 150, 200 i 246 mm (Fig. 2b).

The impedance tests on the reinforcement in concrete specimens began 10 month after their forming. Measurement by EIS technique were performed in a three-electrode system, where the rebar was used as the working electrode *2* with the active area restricted with the insulation *3*. The counter electrode *5* was prepared in a stainless steel mould of 246×96×2 mm, with a centrally located hole to place a reference electrode *6* Cl^-/AgCl,Ag. All three electrodes were connected to the potentiostat *7* Gamry Reference 600. A wet felt was put between the counter electrode and the upper part of concrete specimen, and the electrode was pressed down by concrete load *8* to provide the satisfactory electrical contact. A foil protecting the specimens and the counter electrode provided stabilization of moisture content in concrete during the measurements.

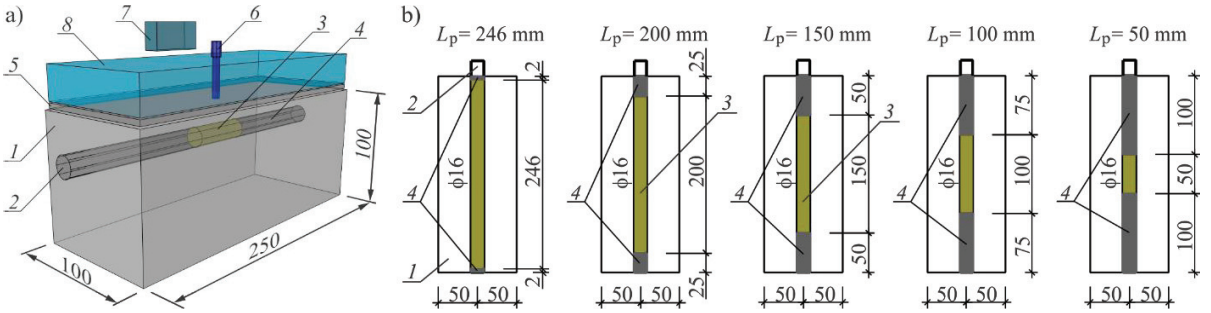

Fig. 2. Test elements: a) in a three-electrode measurement system, b) a method of limiting the polarized area of the reinforcement.

The specimens were immersed up to half of the cover width (ca. 10 mm) in tap water 2 hours before the main tests to increase concrete conductivity. The impedance tests began after 2÷3-hour-long stabilization of potential. The measurements using the EIS technique were performed in the potentiostatic mode applying alternating current at frequencies within the range of 0.01 Hz ÷ 1 MHz, and 10 mV amplitude with regard to the reinforcement stationary potential.

3. Test results

The impedance test results for both *S1* and *S2* series are illustrated at the Nyquist plots (Figs 3e and 3f) and the Bode plots (Figs 3i and 3j). The comparison of both groups of spectra on the complex plane, shows a visible over a 5-fold difference in values of real and imaginary impedance (Figs 3e and 3f). At low frequencies at the Bode plots, reinforcement impedance of *S1* series elements was within quite a broad range of 1.2÷7.4 kΩ (Fig. 3i), whereas for *S2* series elements, it was within a more narrow range of lower values of 0.4÷1.3 kΩ (Fig. 3j). Phase shifts angles in elements of *S1* series show a very clear increasing tendency at decreasing measurement frequency, reaching the level of 19÷26° (Fig. 3i). In *S2* series elements, phase shift angles were within much a larger range of 1÷17° (Fig. 3j). A significant spread of phase shifts angles in *S2* series may indicate slightly diversified electrochemical state of reinforcing steel in individual elements of that series. But at the Nyquist plot (Fig. 3e), distribution shapes of measurement points in *S1* series were typical for steel passivation in concrete. An image of each spectra shows a

distinguishing strongly elongated low-frequency arc which gradually undergoes into a straight line at the lowest frequencies. Shapes of measuring spectra of *S2* series elements (Fig. 3f) are similar to those obtained in *S1* series, however a several times smaller impedance scale may indicate a higher activity of electrode processes on steel in *S2* series. Moreover, a radius of strongly flattened low-frequency arc from the intersection of measuring spectrum and real impedance axis was several times smaller than a radius of analogous arc in *S1* series elements. The conventional diameter of that arc is usually identified with the transfer resistance of charge inversely proportional to corrosion current density in reinforcing steel. The above qualitative evaluation quite unequivocally demonstrates that corrosion current density in reinforcing steel for *S2* series elements should be considerably greater than for *S1* series elements.

Apart from the above electrochemical properties of steel in concrete, also some characteristics related to a specific geometry of tested three-electrode systems are clearly revealed. The effect of spectra scaling is apparent and observed both in elements of *S1* and *S2* series. As may be seen, a spectrum size was decreasing while the length of restricted polarization range L_p was growing. The described phenomena is explained further in the text on the basis of the original 3D model of steel–concrete system.

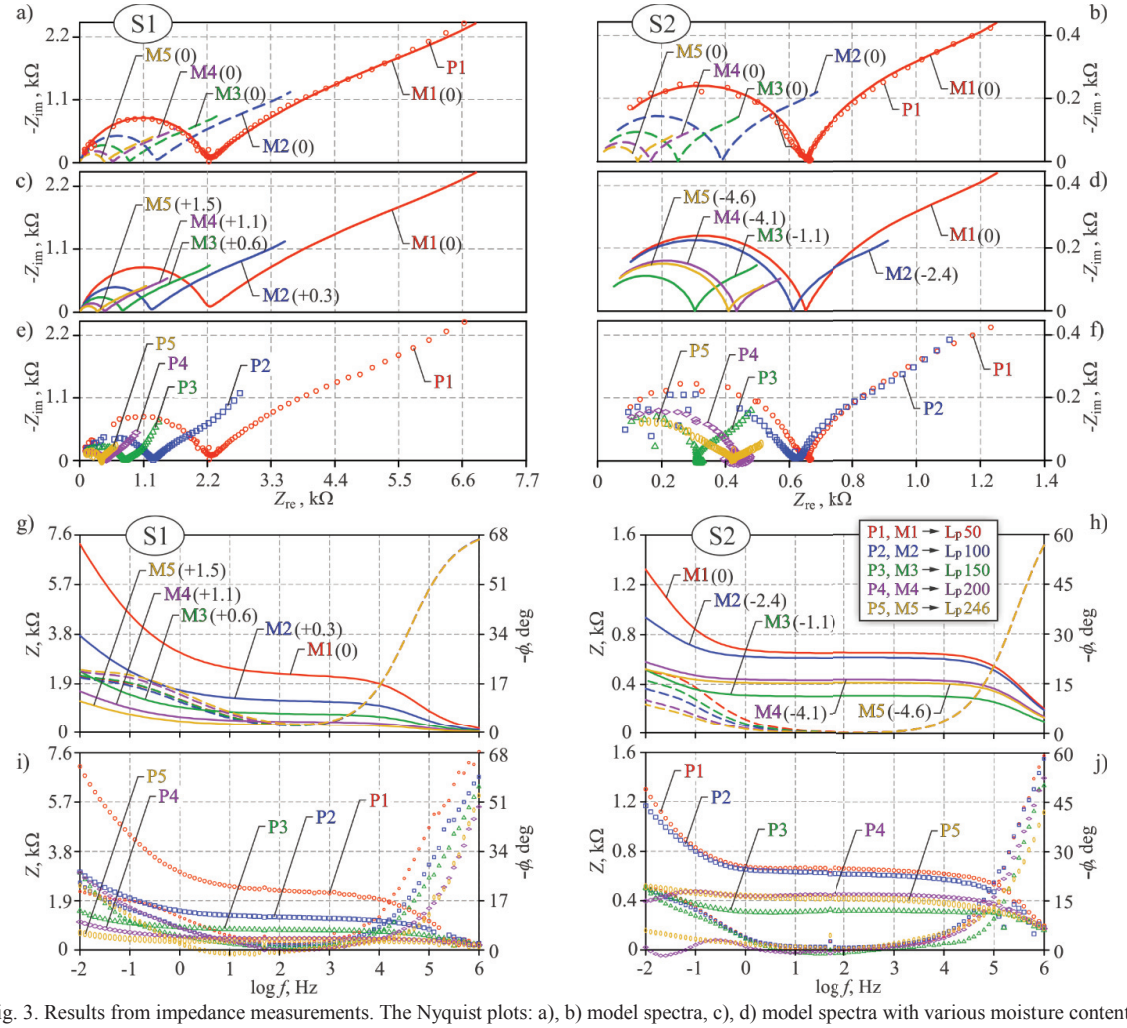

Fig. 3. Results from impedance measurements. The Nyquist plots: a), b) model spectra, c), d) model spectra with various moisture content, e), f) experimental spectra. The Bode plots: g), h) model spectra with various moisture content, i), j) experimental spectra.

4. Assumed 3D model of 'steel-concrete' system

The original 3D model, described in details in the papers by Jaśniok [6] and Jaśniok [8] was used to explain the reasons for shapes of impedance spectra in reinforcing steel with the restricted polarized area in concrete, observed at the Nyquist and Bode plots. The schematic assumptions of a three-dimensional model of steel-concrete system to simulate and analyse the impedance tests on steel in concrete are illustrated in Figs 4a and 4b.

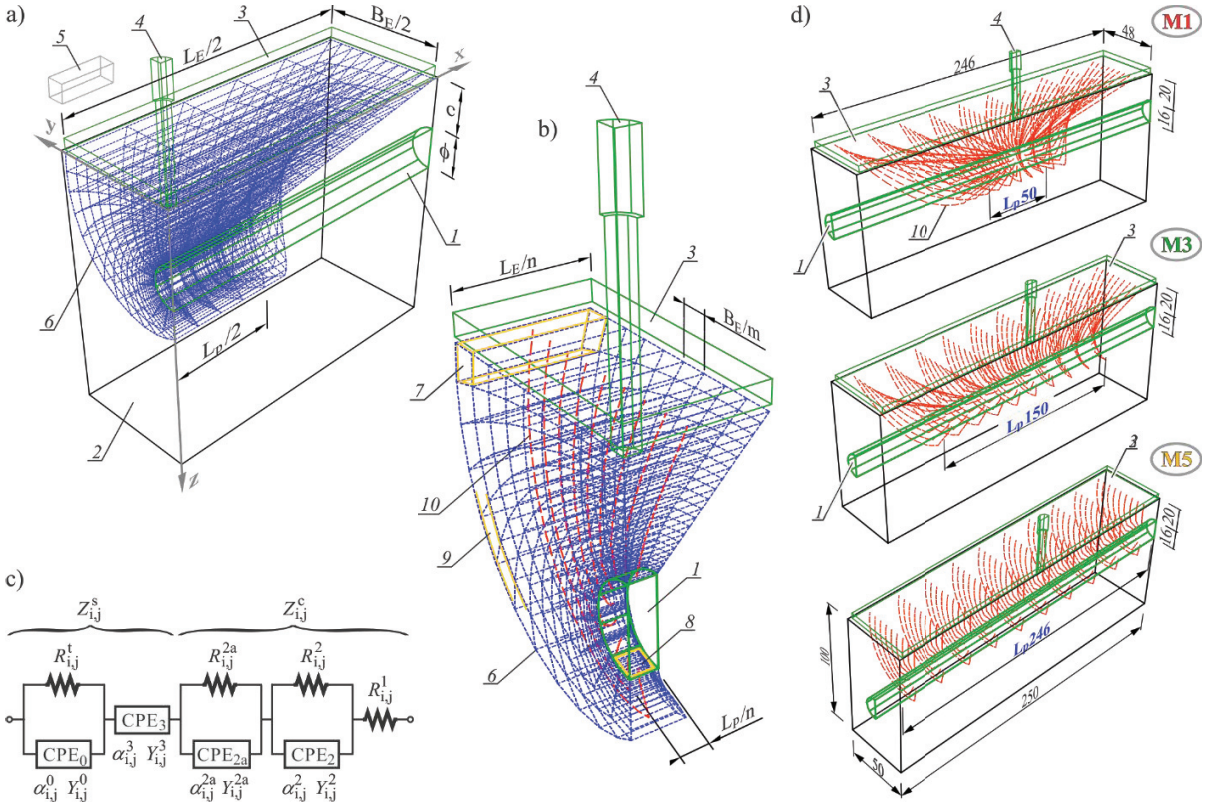

Fig. 4. A 3D model: a) a quarter of the system with two symmetry planes, b) a fragment of the model grid with current lines, c) an elementary equivalent electrical circuit, d) simulated distribution of current lines for three restricted polarization ranges L_p.

The 3D model with reference to tested reinforced concrete specimens has two symmetry planes. For that reason, its quarter is taken into account further in the texts and in Fig. 4a. That model represented a three-electrode system, where a steel bar *1* with a diameter and the length of polarized range of the reinforcement limited to L_p was the working electrode. The bar *1* was embedded in concrete *2*, and the concrete cover width was *c*. The counter electrode *3* was placed on the upper surface of concrete. The electrode was made of sheet with the dimensions $L_E \times B_E$, which covered the whole upper surface of the tested specimen. There was a hole in the geometric centre of the sheet *3* through which the reference electrode *4* was introduced. All three electrodes were connected to the potentiostat *5* controlling the measurement. As soon as the impedance measurement began, electric current was flowing through concrete between the counter electrode *3* and the working electrode *1*. This was the method for revealing the concrete area which actively conducted current between the electrodes *3* and *1*. The spatial grid of nodes *6* was defined to determine the polarized area of bar in the model and concrete volume involved in current conduction. The grid was formed by dividing the model into *n*, *m* and *p* elements towards *x*, *y* and *z* axes respectively. The formulas expressing the grid coordinates of nodes are presented in the paper by Jaśniok [6]. The grid nodes were corners of hexagonal concrete solid elements *7* with volume $V_{i,j,k}$, and steel quadrilateral flat

elements *8* with an area $A^{p}_{i,j}$. Conductive paths *9*, that is elongated curvilinear concrete solids were defined between flat steel elements on the working electrode *1* and the counter electrode *3*. Additionally, theoretical lines of current *10* were determined which corresponded approximately to axes of current paths. For each conductive path, the local geometric factors for concrete $\gamma^{c}_{i,j}$ and steel $\gamma^{s}_{i,j}$ were defined according to the relation (1)

$$\gamma^{s}_{i,j} = \frac{1}{A^{p}_{i,j}} \cdot \frac{\sum_{k=1}^{p} l_{i,j,k}}{\frac{1}{\frac{n}{2}\cdot\frac{m}{2}} \sum_{i=1}^{\frac{n}{2}} \sum_{j=1}^{\frac{m}{2}} \sum_{k=1}^{p} l_{i,j,k}}, \qquad \gamma^{c}_{i,j} = \sum_{k=1}^{p} \frac{l^{2}_{i,j,k}}{\rho^{c} w_{i,j,k} V_{i,j,k}} \ . \tag{1}$$

In the equations (1), the parameter $l_{i,j,k}$ defines the length of the theoretical line of current in the solid element, $w_{i,j,k}$ – moisture content by mass in solid element, and ρ^{c} – concrete density. Local geometric factors were used to define the expressions for the global geometric factors for concrete γ^{c} and steel γ^{s}, which can be calculated from the equations (2) taking into account two symmetry planes of the modelled system.

$$\gamma^{s} = \frac{1}{\sum_{i=1}^{\frac{n}{2}} \sum_{j=1}^{\frac{m}{2}} \frac{4}{\gamma^{s}_{i,j}}}, \qquad \gamma^{c} = \frac{1}{\sum_{i=1}^{\frac{n}{2}} \sum_{j=1}^{\frac{m}{2}} \frac{4}{\gamma^{c}_{i,j}}}. \tag{2}$$

The identical elementary equivalent circuit (Fig. 4c) was assigned to each conductivity path. The circuit was composed of resistors of $R_{i,j}$ resistance and the constant phase elements CPE defined by $Y_{i,j}$ and $\alpha_{i,j}$ parameters. A part of the system typical for steel impedance $Z^{s}_{i,j}$ and a part referring to concrete impedance $Z^{c}_{i,j}$ could be identified in the equivalent circuit. The total impedance of steel–concrete model system was defined by the expression (3), where the parameters R^{s}, Y^{s} characterized steel properties with reference to the area unit, and the parameters R^{c}, Y^{c} characterized concrete properties per volume unit. The parameters α^{c} and α^{s} are dimensionless.

$$Z = \frac{1}{\sum_{i=1}^{\frac{n}{2}} \sum_{j=1}^{\frac{m}{2}} \left(\frac{4}{Z^{c}_{i,j} + Z^{s}_{i,j}} \right)}, \qquad \begin{aligned} &Z^{c}_{i,j} = Z^{c}_{i,j}\left(R^{c}_{i,j}, Y^{c}_{i,j}, \alpha^{c}_{i,j}\right), \quad R^{c}_{i,j} = R^{c} \cdot \gamma^{c}_{i,j}, \quad Y^{c}_{i,j} = \frac{Y^{c}}{\gamma^{c}_{i,j}}, \quad \alpha^{c}_{i,j} = \alpha^{c}, \\ &Z^{s}_{i,j} = Z^{s}_{i,j}\left(R^{s}_{i,j}, Y^{s}_{i,j}, \alpha^{s}_{i,j}\right), \quad R^{s}_{i,j} = R^{s} \cdot \gamma^{s}_{i,j}, \quad Y^{s}_{i,j} = \frac{Y^{s}}{\gamma^{s}_{i,j}}, \quad \alpha^{s}_{i,j} = \alpha^{s}. \end{aligned} \tag{3}$$

5. The analysis of impedance tests using the '3D' model

The observed changes in impedance spectra shapes caused by a change in the polarized area of the steel bar restricted by insulation can be predicted by means of the above 3D model of steel–concrete system. For that reason, in 1st stage the so called initial spectra were selected among all spectra obtained for the specimens from *S1* and *S2* series (Figs 3a and 3b). The initial spectra *P1* were obtained at the most restricted range of reinforcement polarization L_{p} = 50 mm. Then, the conventional iterative analysis was performed to adjust the model spectra to the experimental ones according to the equivalent circuit from Fig. 4c, the results of which are shown in first column of Table 1. In 2nd stage, all resistance values referring to concrete (r^{1}, r^{2}, r^{2a}) were divided and values of the parameters y^{2}, y^{2a} were multiplied by the global geometric factors for concrete γ^{c}. The similar calculations were made for parameters referring to steel, by multiplying or dividing them by the global geometric factors for steel γ^{s}. The parameters α were not subjected to any calculations. The values presented in 2nd column of Table 1 are the

unit parameters of the 3D model, and when substituted into the relations (3), they allow us to predict shapes of analysed impedance spectra at, inter alias, changing polarized area of the reinforcement. The papers by Jaśniok [6] and Jaśniok [8] demonstrated that the 3D model also correctly predicted the tendencies towards changes in spectra shapes at changing diameter of the rebar and the concrete cover width *c*.

Table 1. The results from analysing impedance spectra of reinforcing steel in concrete.

	Parameters of initial spectra with no reference to the material area or volume				Unit parameters of the 3D model common for 5 spectra of *S1* and *S2* series			
		S1	*S2*			*S1*	*S2*	
concrete	r^1 =	0	0	Ω	R^1 =	0	0	Ω·cm
	r^2 =	4.543	0.639	kΩ	R^2 =	21.18	3.576	kΩ·cm
	r^{2a} =	1.154	1.293	kΩ	R^{2a} =	5.380	7.235	kΩ·cm
	y^2 =	3.058	80.92	nF·s$^{\alpha-1}$	Y^2 =	0.656	14.46	nF·s$^{\alpha-1}$/cm
	α^2 =	0.816	0.752		α^2 =	0.816	0.752	
	y^{2a} =	1775	284.0	nF·s$^{\alpha-1}$	Y^{2a} =	380.7	50.76	nF·s$^{\alpha-1}$/cm
	α^{2a} =	0.583	0.669		α^{2a} =	0.583	0.669	
steel	y^3 =	2112	4260	μF·s$^{\alpha-1}$	Y^3 =	26.03	52.51	μF·s$^{\alpha-1}$/cm^2
	α^3 =	0.269	0.077		α^3 =	0.269	0.077	
	y^0 =	4302	3090	μF·s$^{\alpha-1}$	Y^0 =	53.03	380.9	μF·s$^{\alpha-1}$/cm^2
	α^0 =	0.641	0.830		α^0 =	0.641	0.830	
	r^t =	4.804	1.510	kΩ	R^t =	389.7	122.5	kΩ·cm^2

In 3rd stage, the parameter L_p = 50, 100, 150, 200 and 246 mm was defined in the 3D model using the original software and the predicted distributions of impedance spectra were generated (dashed lines in Figs 3a and 3b). In the final stage of the analysis, the distributions of model spectra were corrected (solid lines in Figs 3c, 3d, 3g and 3h) by the iteratively selected value of the so called averaged theoretical moisture content $w_{mid} = w_{i,j,k}$, for which the adjustment of model spectra to the experimental ones (distribution of points) was the most satisfactory. The value of optimal theoretical moisture content illustrated in the diagrams in Fig. 3 was shown as a difference of Δw_{mid} in moisture content, measured by a dielectric hygrometer, between the specimens for which the initial spectra were assumed and the specimen for which the spectrum shape was predicted. In the diagrams in Fig. 3, the value Δw_{mid} was included in brackets at the symbol *M* denoting the model spectrum. For example, the symbol *M5*(+1.5) meant the model spectrum *M5* adjusted to the experimental spectrum *P5* obtained for the theoretical moisture content larger by 1.5% than the model initial spectrum *M1*(0).

6. Conclusions

By evaluating the test and analysis results shown in Fig. 3, it can be found that the 3D model quite correctly represents the tendencies towards changes in impedance spectra shapes in the function of changing active area of the (reinforcement) working electrode. Quite high values of an increase in theoretical moisture content in concrete Δw_{mid} mainly result from comparing the impedance measurements performed on the unrelated specimens with originally different moisture content in concrete.

According to the previous tests by Jaśniok [5] and Jaśniok [6], the low-frequency radius of arc typical for steel was distinctly shortened at the increasing area of the working electrode (caused by a change in a diameter or length of the rebar). In the analysed tests, the increased polarized area at the constant diameter of rebar also resulted in the clearly reduced radius of the spectrum arc (Figs 3e and 3f). Moreover, the significant changes in the shape were observed for the high-frequency part of the spectrum typical for concrete. In that case, the conventional diameter of the high-frequency flattened semicircles was reduced (Figs 3e and 3f) at the increasing polarized area of the reinforcement. The described trends were found in the specimens from both *S1* and *S2* series.

The discussed tendencies can be explained by the previously mentioned equations (1)÷(3) describing the main assumptions of the 3D model. The smaller the active area of the working electrode is, the higher the value of the local geometric factor for steel $\gamma^{s}_{i,j}$ is. The increasing factor $\gamma^{s}_{i,j}$ results in an increase in steel impedance $Z^{s}_{i,j}$, which for simplification is expressed here as the parameter $R^{s}_{i,j}$. If $Z^{c}_{i,j}$ impedance is finally neglected in the equation (3), then the total impedance of the system would be the greatest at the smallest polarized area of the steel bar (cf Figs 3c and 3d). For concrete, the longest the conductivity path is, the higher the value of the local geometric factor for concrete $\gamma^{c}_{i,j}$ is. In this way the impedance of concrete $Z^{c}_{i,j}$ simplified to the parameter $R^{c}_{i,j}$ is higher for longer current paths. As it was shown in the simulated distribution of current lines according to the 3D model (Fig. 4d), a number of elongated current lines (which correspond approximately to axes of current paths) increases at reduced active area of the working electrode. It means that the total impedance of the system, at neglected impedance of steel $Z^{s}_{i,j}$ for simplification, will be decreasing at increasing polarized area of the reinforcement (cf Figs 3c and 3d).

The reasons for observed changes in the spectra shapes, which are not caused by altered electrochemical properties of the steel–concrete system, but only refer to a change in the active area of the working electrode, explained on the basis of the 3D model can be used as a significant hint to interpret impedance tests on steel in concrete.

References

[1] Feliu S., Gonzalez JA, Escudero ML, Feliu Jr. S, Andrade MC. Possibilities of the Guard Ring for Electrical Signal Confinement in the Polarization Measurements of Reinforcements. *Corrosion*, 1990; 46: 1015-1020.

[2] Feliu V, Gonzalez JA, Andrade C, Feliu S. Equivalent circuit for modelling the steel-concrete interface. I. Experimental evidence and theoretical prediction. *Corros Sci* 1998; 40:975-993.

[3] Ford SJ, Shane JD, Manson TO. Assignment of features in Impedance Spectra of the Cement-Paste/Steel System, *Cement Concrete Res* 1998; 28:1737-1751.

[4] Gonzalez JA, Benito M, Feliu S, Rodriguez P, Andrade C. Suitability of Assessment Methods for Identifying Active and Passive Zones in Reinforced Concrete, *Corrosion* 1995; 51:145-152.

[5] Jaśniok M. Examining and Modelling the Influance of Lenghts of Rebars in Concrete to Shapes of Impedance Spectra. *Cem Wapno Beton* 2012; Special Issue:30-34.

[6] Jaśniok M. Investigation and Modelling of the Impact of Reinforcement Diameter in Concrete on Shapes of Impedance Spectra, *Procedia Engineering* 2013; 57:456-465.

[7] Jaśniok T, Jaśniok M, Zybura A. Studies on corrosion rate of reinforcement in reinforced concrete water tanks. *Ochr. Przed Koroz.* 2013; 56:227-234.

[8] Jaśniok M.. Analysis of the thickness of steel rebars cover in concrete effect on the impedance spectra in the reinforced concrete. *Cem Wapno Beton* 2014; 1:46-58.

[9] Jaśniok T, Jaśniok M,. Electrochemical tests on corrosion of the reinforcement in reinforced concrete silos for cement. *Ochr. Przed Koroz.* 2014; 57:225-229.

[10] Jaśniok T, Słomka-Słupik B, Zybura A. The concrete reinforcement chloride corrosion, immediately after its initiation. *Cem Wapno Beton* 2014; 3:158-165.

[11] Lemoine L, Wenger F, Galland J. Study of the Corrosion of Concrete Reinforcement by Electrochemical Impedance Measurement. In: Berke NS, et al. editors. *Corrosion Rates of Steel in Concrete, ASTM STP 1065*, Philadelphia: American Society for Testing and Materials; 1990, p. 118-133.

[12] Macdolnad DD, Mckubre MCH, Urquidi-Macdonald M. Theoretical Assessment of AC Impedance Spectroscopy for Detecting Corrosion of Rebar in Reinforced Concrete. *Corrosion* 1988; 44:2-7.

[13] Matsuoka K, Kihira H, Ito S, Murata T. Corrosion Monitoring for Reinforcing Bars in Concrete. In: Berke NS, et al. editors. *Corrosion Rates of Steel in Concrete, ASTM STP 1065*, Philadelphia: American Society for Testing and Materials; 1990, p. 103-117.

[14] Saravanan K, Sathiyanarayanan S, Muralidharan S, Syed Azim S, Venkatachari G. Performance evaluation of polyaniline pigmented epoxy coating for corrosion protection of steel in concrete environment. *Progress in Organic Coatings* 2007; 59:160-167.